Wiley
Advances in Meteorology
Volume 2025, Article ID 2584412, 17 pages
https://doi.org/10.1155/adme/2584412

WILEY

Research Article

Observation and Numerical Simulation of a Microburst Encounter by an Arriving Aircraft at Hong Kong International Airport During Intense Convective Weather on August 14, 2025

M. L. Chong,[1] H. M. Chen,[2] H. Y. Yeung,[1] P. Cheung,[1] X. M. Shi,[2] S. K. Lai,[1] Y. H. He,[1] and P. W. Chan[1]

[1]*Hong Kong Observatory, Hong Kong, China*
[2]*Hong Kong University of Science and Technology, Hong Kong, China*

Correspondence should be addressed to P. W. Chan; pwchan@hko.gov.hk

Received 12 September 2025; Revised 16 October 2025; Accepted 12 November 2025

Academic Editor: Zhengyu Xia

A microburst encounter near the ground was documented for the first time at Hong Kong International Airport (HKIA). Analysis of the flight data for the concerned aircraft revealed that it passed through at least three small vortices within the band of heavy rain. Most notably, the aircraft experienced an updraft–downdraft vertical velocity couplet when encountering the microburst, the corresponding eddy dissipation rate (EDR) reached approximately 0.6–0.8 $m^{2/3} s^{-1}$. The weather radar data during the event was analyzed, through calculating the EDR field and identifying the descending radar reflectivity cores in the vertical cross sections across strong convection. The radar observations were generally consistent with aircraft data, and the Terminal Doppler Weather Radar (TDWR) provided timely and accurate microburst alerts. Finally, the performance of a convection-permitting numerical weather prediction (NWP) model is investigated regarding this event. The model was found to capture the location of the downdraft reasonably well, although the magnitude of the vertical velocity was weaker than that observed in actual conditions. The EDR from the model output agreed with the flight and radar data. From this example, it appears that the high-resolution NWP model has the potential to provide early warnings of downdrafts and turbulence, thereby safeguarding airport operations.

1. Introduction

Downdrafts are associated with the evaporation of precipitation in convection that cools surrounding air, causing cooler and unsaturated air to descend [1, 2]. Intense downdrafts are more favorable with a high environmental lapse rate, close to dry adiabatic [3]. Fujita [4, 5] defined microburst as a downburst with a scale of 4 km or smaller. Microbursts bring about severe low-level windshear that can be hazardous to aircraft, particularly arrivals, and have been the culprit of many aircraft accidents [6]. At the Hong Kong International Airport (HKIA), the Hong Kong Observatory (HKO) operates a Terminal Doppler Weather Radar (TDWR) at Brothers Point to provide detection-based, timely microburst alerts to the aircraft. As the airport is rather busy and microburst events are mostly short-lived, usually lasting for about several minutes [7], aircraft may still approach when microbursts could potentially occur, depending on airline policies and judgement of the pilot. Missed approach could be conducted at a lower altitude as deemed necessary.

Previously, observational studies have been conducted on microbursts occurring inside and around the HKIA by comparing weather radar-retrieved wind fields with flight data collected onboard aircraft. In these studies, the arriving aircraft made a missed approach, and the microburst was encountered at a higher altitude. The present study is the first of its kind to document the observational aspect of a microburst spreading to the ground and encountering an aircraft with a missed approach. Aircraft data provide a unique opportunity to study the structures of microbursts in the region. The

detection and alerting of microbursts by weather radars have also been documented.

The HKO recently introduced an atmosphere-ocean-wave coupled numerical weather prediction (NWP) model, also known as UWIN-CM, with convection resolution (innermost domain with a spatial resolution of 1.33 km) for heavy rain forecasts in the Pearl River Estuary region. This mesoscale-to-microscale model is driven by a global artificial intelligence model, specifically Pangu, based on the European Centre for Medium-Range Weather Forecasts (ECMWF) analysis. The performance of this model in capturing the intense convection associated with the microburst and turbulence intensity, the eddy dissipation rate (EDR) to be specific, is also studied.

2. Synoptic Setup and Weather Station Observations

The event occurred on the morning of August 14, 2025, when Tropical Cyclone Podul had already made landfall and moved westwards north of Hong Kong. The isobaric chart at the surface at 00 UTC on that day (8 a.m. in Hong Kong time, with HKT = UTC + 8 h) is shown in Figure 1a. The cyclonic vortices at various levels of the troposphere, in association with Podul, brought heavy rains to Hong Kong.

Surface observations (Figure 1b) showed a moderate southwesterly flow prevailed over the western part of the territory in the morning. Over the seas east of HKIA, there was convergent northerly flow, associated with cooler air plunging and spreading on the ground from higher altitudes of the thunderstorms; more observations at that time will be discussed subsequently.

The analysis of the radiosonde data at 00 UTC on August 14, 2025 and its comparison with climatological data is given in Figure 1c. Various parameters were derived from the radiosonde data, including dynamical factors (first column), moisture parameters (second and third columns), instability parameters (fourth column), and other parameters (fifth column). The radiosonde data was compared with the climatology of July to September in 2001–2020. When the parameter based on the radiosonde data reaches a relatively high or extreme value, the corresponding box will be highlighted in red or purple, respectively. In the concerned radiosonde data in this study, only a few values reached high or extreme values compared to climatology in the analysis, and the only noteworthy parameter was the precipitable water vapor (PWV), which reached a high value of 68.5 mm. The *K* index was close to 40; however, the convective available potential energy (CAPE) was not particularly high. Synoptic and mesoscale patterns (e.g., the relatively low value of the 500 hPa geopotential height associated with the vortex of Podul) and abundant moisture could be the two significant factors contributing to the occurrence of heavy rain.

3. Aircraft Observations

An aircraft arriving at the northern runway of the HKIA from the east conducted a missed approach at approximately 23:40 UTC August 13, 2025. It then encountered a microburst at approximately 23:41 UTC, when the aircraft was around 4000 ft above sea level, overhead of the touchdown zone. The data for the significant part of the flight are shown in Figure 2a. The en route EDR was calculated using an in-house developed Python-based algorithm based on the methods of Haverdings and Chan [8] and the EDR2W of Kim et al. [9], which are referred to as the NLR and Spectrum. The vertical wind was derived from Huang et al. [10]. For both NLR and Spectrum, the peak EDR reached approximately 0.6–0.8 $m^{2/3}\ s^{-1}$, indicating severe turbulence. Around the time of the peak EDR, the vertical velocity showed an updraft–downdraft couplet, or more precisely, one updraft followed by two downdrafts. The vertical velocity pattern generally agreed with the conceptual model of microburst occurring along a glide path [6] and past measurements of research aircraft [11]. Comparing with radar observations (e.g., Figure 3), the aircraft first encountered the updraft associated with the air spreading out on the ground (also consistent with the observation in Figure 1b), and then encountered two regions of descending air (the central radar reflectivity core highlighted in a red ellipse in Figure 3a, and another, secondary to the east of it, highlighted in a black ellipse).

From the horizontal wind speed and wind direction time series, the aircraft experienced three encounters of tiny cyclones during that part of the flight, each time with a rotating wind direction and a relatively lower horizontal wind speed. Figure 2a also displays the aircraft's altitude, which is magnified in Figure 2b, highlighting the period close to the missed approach. The windshear detected from the aircraft data is highlighted in gray. The aircraft encountered a negative shear of approximately 16 knots, specifically a headwind of +4 knots followed by a tailwind of −12 knots. The windshear is consistent with the conceptual model of a microburst, of which airflow diverges when plunged to the ground, and this microburst could be the "secondary" one in Figure 3a.

4. Radar Observations

Figure 4a shows a 0.1-degree plan position indicator (PPI) scan from a long-range S-band surveillance weather radar in Hong Kong, located at Tate's Cairn. The EDR was calculated from the spectrum width of another C-band weather radar located approximately 50 km west of HKIA, using the method described by Chan et al. [12]. Owing to the distance from the radar, only the EDR at a height of approximately 2 km above sea level was considered. The peak value near HKIA is about 0.6 $m^{2/3}\ s^{-1}$, consistent with flight data (Figure 2a).

The three-dimensional wind field during the event was reconstructed using multiple Doppler weather radar datasets, including the Qiu Yu Tan radar in Shenzhen, Zhuao radar in Zhuhai adjacent to Macau, and the Tai Mo Shan and Sha Lo Wan radars in Hong Kong, along with NWP model outputs as initial guess. This reconstruction utilized the Python library PyDDA [13], which employs a wind retrieval algorithm based on 3D variational data assimilation (3DVAR). Examples of convection cases analyzed with this method can be found in Lau and Chan [14]. This event was well-covered by the radar

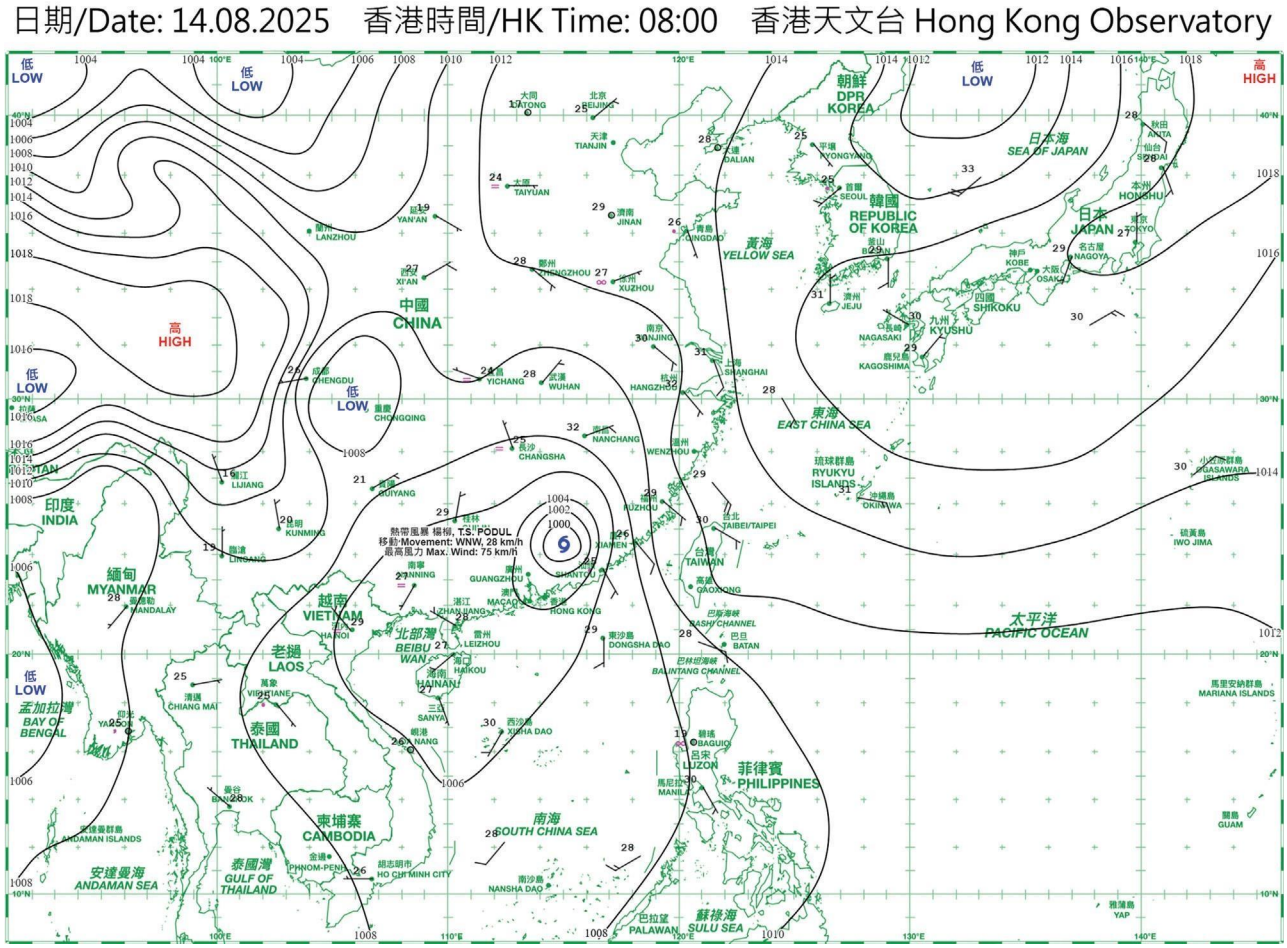

(a)

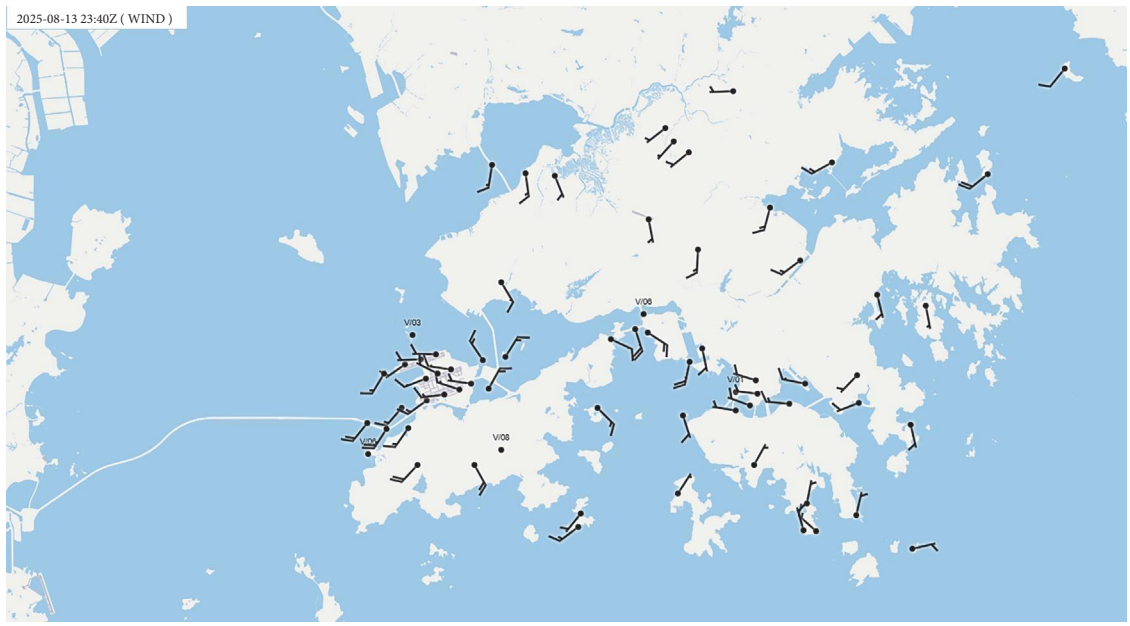

(b)

FIGURE 1: Continued.

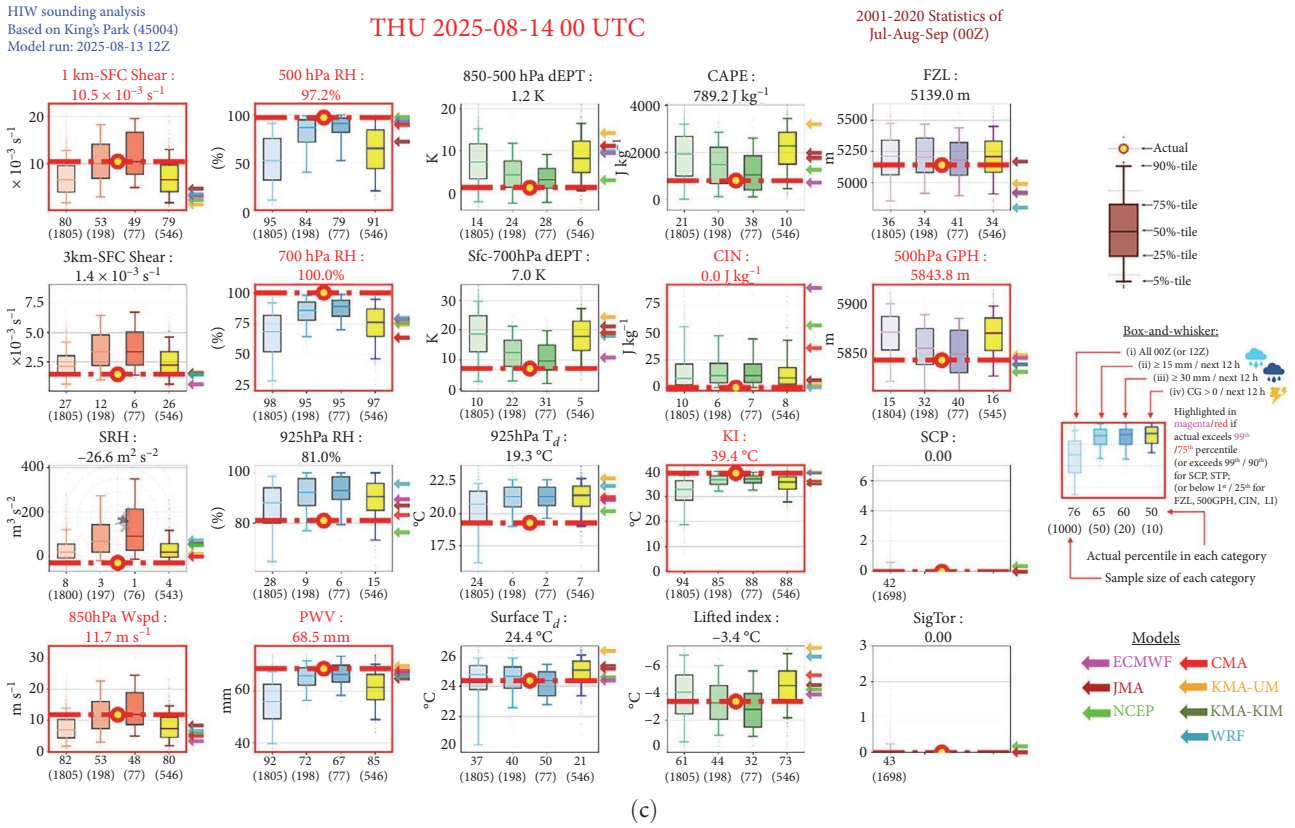

(c)

FIGURE 1: Conventional in situ weather measurement and analysis around 00 UTC of August 14, 2025. (a) Surface weather chart at 00 UTC of August 14, 2025; (b) winds observed by surface-based anemometers over Hong Kong at 23:40 UTC of August 13, 2025; (c) weather indices and quantities favorable for convections based on radiosonde at King's Park (45004) at 00 UTC of August 14, 2025. CAPE, convective available potential energy; CIN, convective inhibition; dEPT, difference of equivalent potential temperature; FZL, freezing level; GPH, geopotential height; KI, *K* index; PWV, precipitable water vapor; SCP, supercell composite parameter; SigTor, significant tornado parameter; SRH, storm relative helicity; T_d, dew point temperature.

network from different directions and within several tens of kilometers. The 2 km wind field at the time of the event is shown in Figure 5a. At the location of the microburst encounter, there was a troughing flow at this height in association with an intense radar echo to the northwest. A vertical cross section was made along the runway, and the resulting wind field projected onto this cross sectional plane is shown in Figure 5b. Descending motion was observed at a height of 2 km at the location of the microburst encounter. A slight updraft is observed to the east and west. However, due to the relatively high elevation of the S-band weather radars in Hong Kong (located at the mountains at 500–1000 m above sea level), wind fields below approximately 2 km are not available. Lower level observations were provided by the C-band TDWR, which covered only the HKIA region.

The TDWR Doppler velocity at the time of the event is shown in Figure 6. There are two regions of diverging flow (green-yellow couplet, with cool color towards the radar and warm color away from the radar) approaching the northern runway of the HKIA from the east, one of which just over the east of the northern runway. The microburst encountered by the aircraft in Figure 2a corresponds to the location of the diverging flow.

A sequence of vertical cross sections by the TDWR towards its west was plotted by combining multiple PPI scans at different scan angles to analyze the vertical structure and evolution of the microburst event in Figure 3. In Figure 3a, the primary radar reflectivity core, which decreases with time, is highlighted in red. This is believed to be a major microburst that aircraft encountered on the runway. Another region of descending radar reflectivity to the east, highlighted in black, is considered secondary. These two descending cores may give rise to two downward motions as recorded by the aircraft's vertical velocity data. The primary central descending reflectivity core also had a clear signature of diverging airflow on the ground, as highlighted in red in Figure 3b.

5. Microburst Detection

Microbursts were detected from the Doppler velocity and reflectivity data from the TDWR using a proprietary algorithm, with some technical details provided by Chan et al. [15]. The

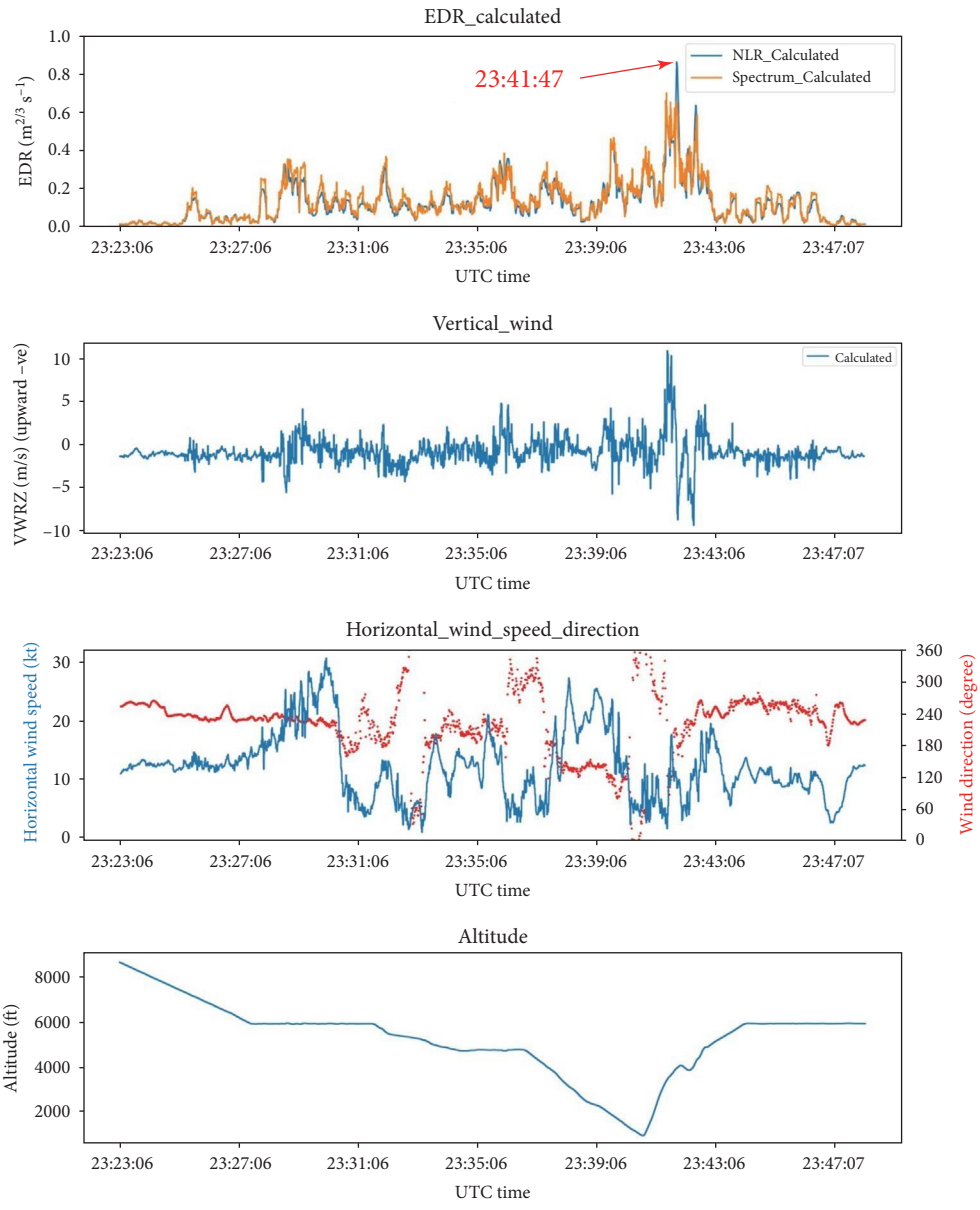

(a)

Figure 2: Continued.

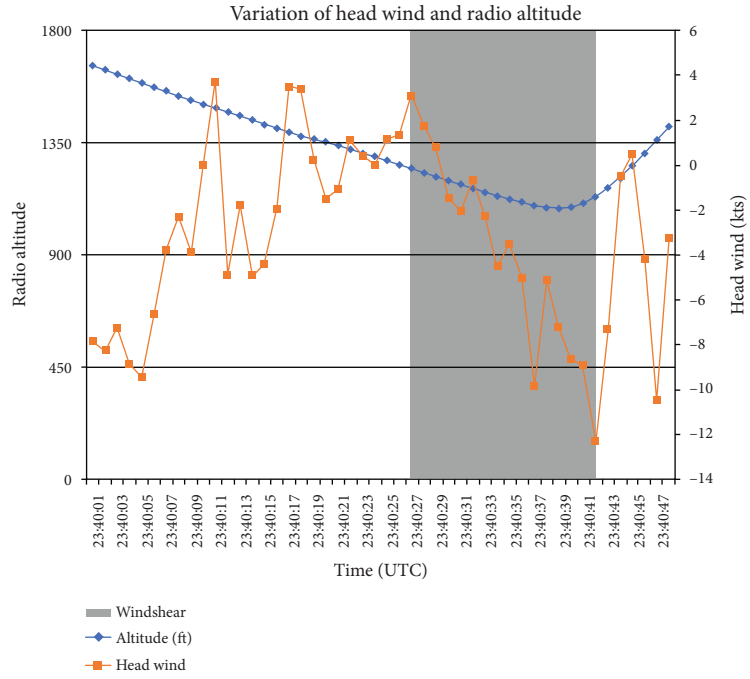

(b)

FIGURE 2: (a) Analyzed flight data of the aircraft that encountered a microburst with EDR and vertical velocity; and (b) its derived headwind profile and windshear during the missed approach.

microburst alerts were relayed to HKO's Windshear and Turbulence Warning System (WTWS) for integration and display. A snapshot of the display during the event is shown in Figure 7. A microburst alert of −35 knots headwind change covered the center and northern runways, and waters north of the HKIA, the location of microburst agrees with flight data from the aircraft. Additionally, there are red polygons indicating windshear alerts from other algorithms and equipment used by the WTWS.

6. Numerical Simulation Result

The performance of short-range forecast of UWIN-CM for the microburst event is evaluated. The 6-h forecast of rainfall and surface wind field based on the model run initialized at 18 UTC on August 13, 2025 is shown in Figure 8a. The rainfall pattern over Hong Kong is quite similar to weather radar observations (Figure 4a). At the 925 hPa level (Figure 8b), a strong positive vorticity (colored red) was forecast over the western part of Hong Kong along the southern edge of the circulation of Podul. This contributed to the occurrence of heavy rains in a synoptic scale.

Plots with smaller domains were generated at lower levels to examine the mesoscale features resolved by the model. A snapshot of the 980 hPa-level horizontal wind field, divergence, and vertical wind for the same T + 6 h forecast is shown in Figure 9. Although we may not expect the downburst associated with intense convection to occur at the exact location as the actual observation, there is a region of significant downward motion over the northeastern waters of the HKIA, which is reasonably near the downdraft location experienced by the aircraft.

Comparing the vertical wind presented in Figures 9b and 10, it was noticed that the model generally shows weak updraft and downdraft motions near the surface, and vertical motion is generally stronger at higher layers, say at 850 hPa. The magnitude of the downward motion at 925 hPa is on the order of 3 m s^{-1}, which is relatively small compared with the actual observations in Figure 2a, but is already considered to be sufficiently close to the aircraft data, given that radar data assimilation has not been performed in running UWIN-CM. This mesoscale/microscale model is a dynamic downscaling of a global artificial intelligence-based model. There is an exception that upward motion was particularly strong in the cross section under forced lifting, when surface northerlies encountered the terrain of Lantau Island near 22.30°N 113.96°E. Referring back to the downdraft over the northeast of HKIA, a descending column appears at the location of the 980 hPa downdraft, accompanied by upward motion to its north and south. The downdraft seems to occur between two areas of significant convection. The detection of such a downdraft may be helpful in timely alerting of windshear and even microbursts, which is basically a detection based on the existing suite of meteorological equipment. From the horizontal cross section (Figure 10a), upward motions are also shown to the east and west of the downdraft. This agreed with the radar-retrieved wind field shown in Figure 5b.

The EDR at low levels was also calculated from the model outputs as per the Sub-Filter-Scale Reconstruction method of

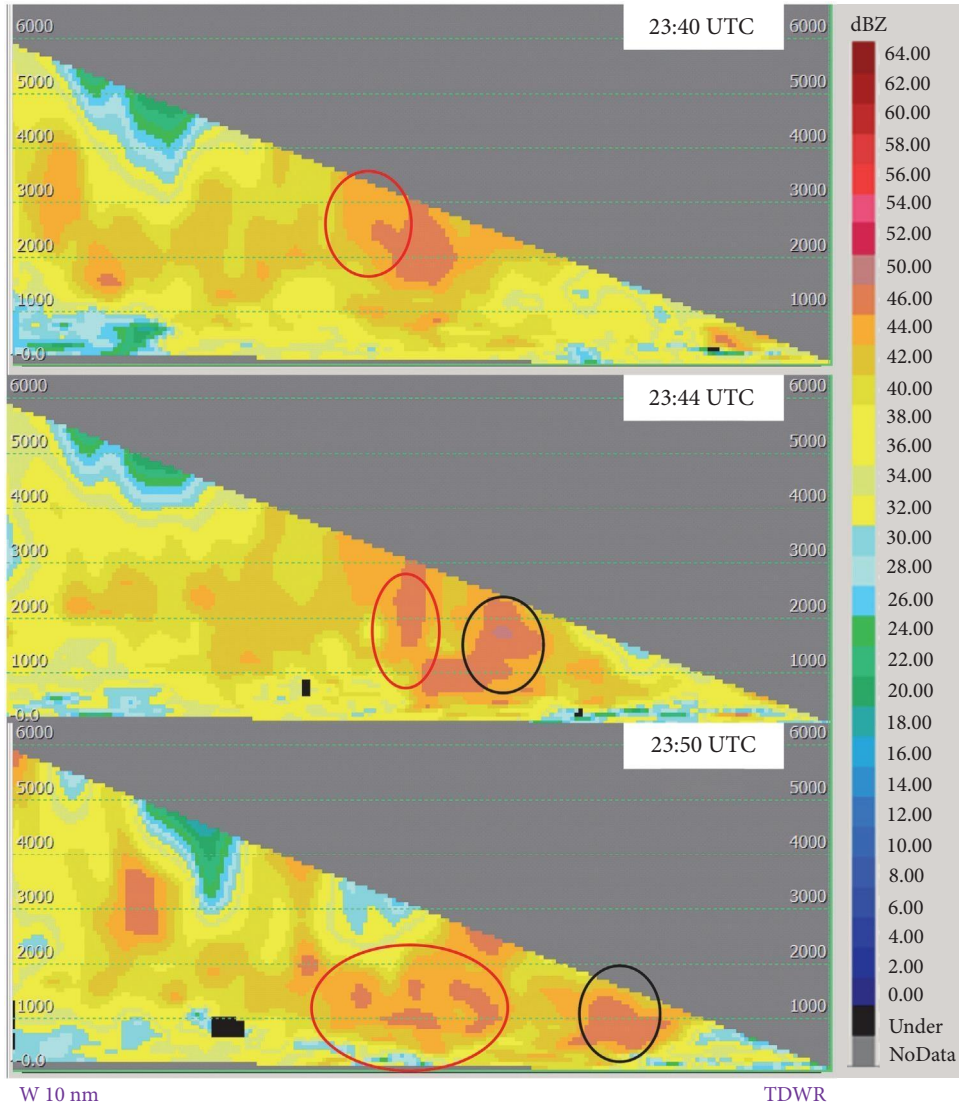

(a)

Figure 3: Continued.

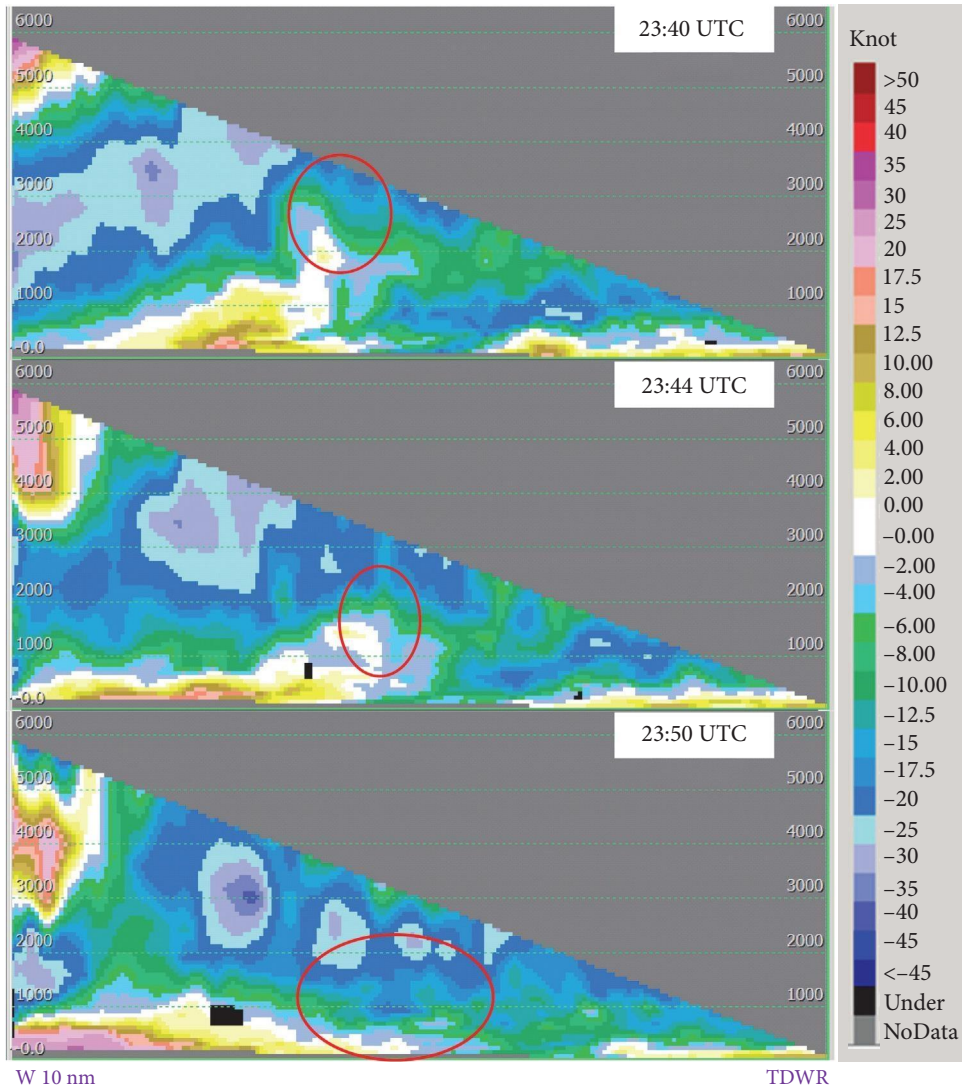

(b)

Figure 3: A sequence of vertical cross sections of (a) reflectivity and (b) Doppler velocity towards the west of the TDWR upto 10 nautical miles at 23:40, 23:44, and 23:50 UTC.

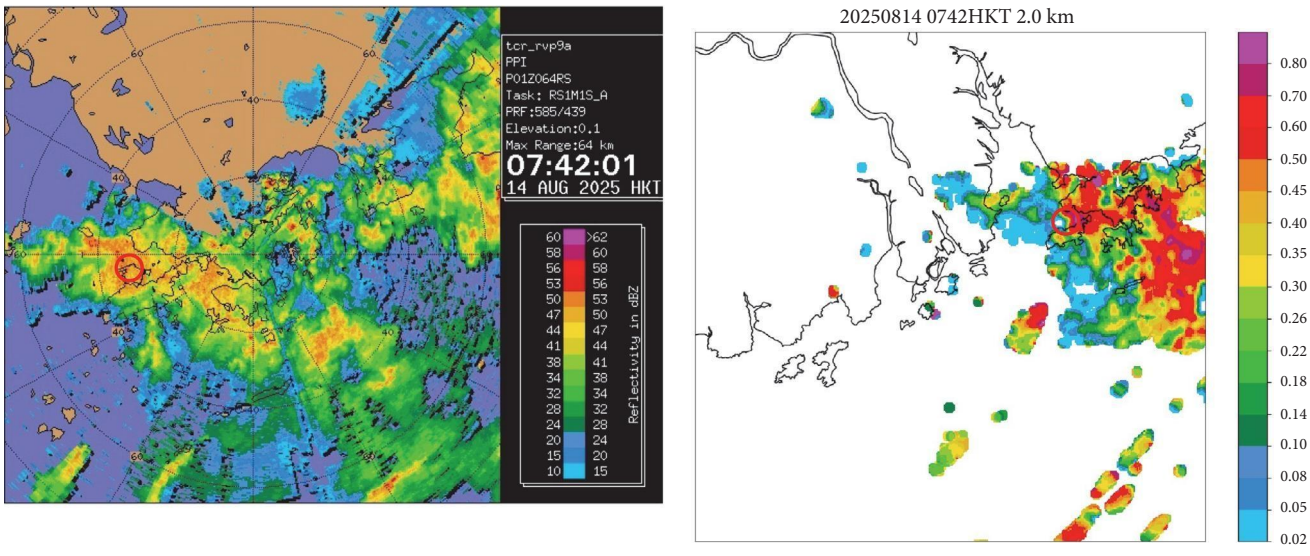

(a) (b)

Figure 4: (a) Reflectivity of long-range radar at Tate's Cairn at a 0.1-degree PPI scan at 23:42 UTC on August 13, 2025; (b) 2 km height composite EDR image from another weather radar at the same time. The small red circles in both subfigures indicate the location where the aircraft encountered severe turbulence.

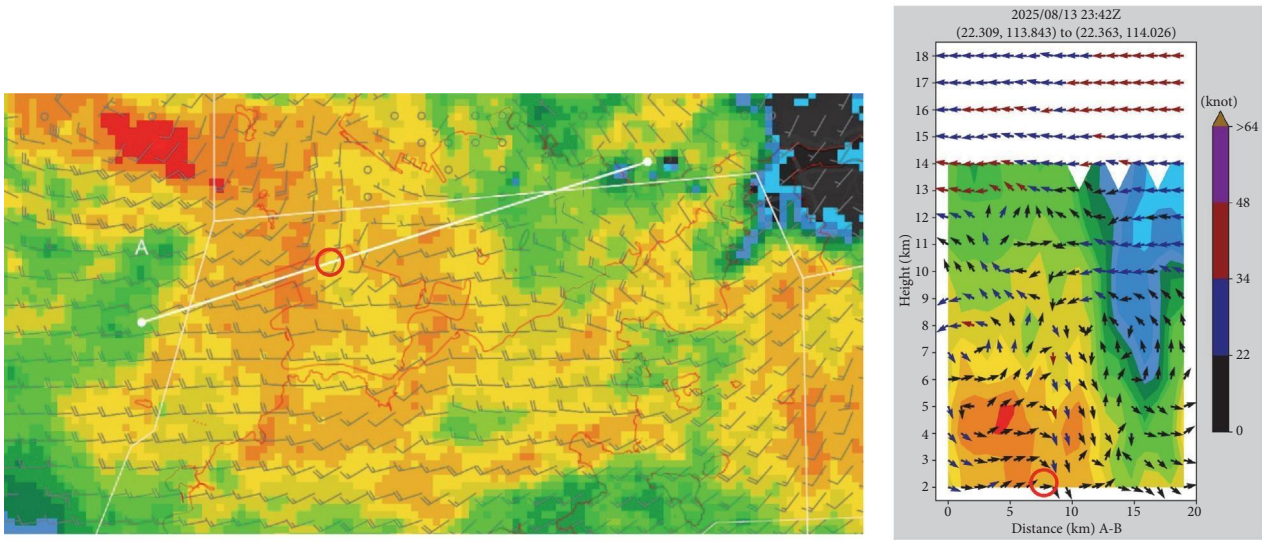

(a) (b)

FIGURE 5: The three-dimensional reflectivity (same scale as Figure 4a) and wind field from multiple Doppler weather radar data at 23:42 UTC, (a) is the horizontal field and (b) is the cross section along the white line in (a). The small red circle on the line indicates the location where the aircraft encountered severe turbulence.

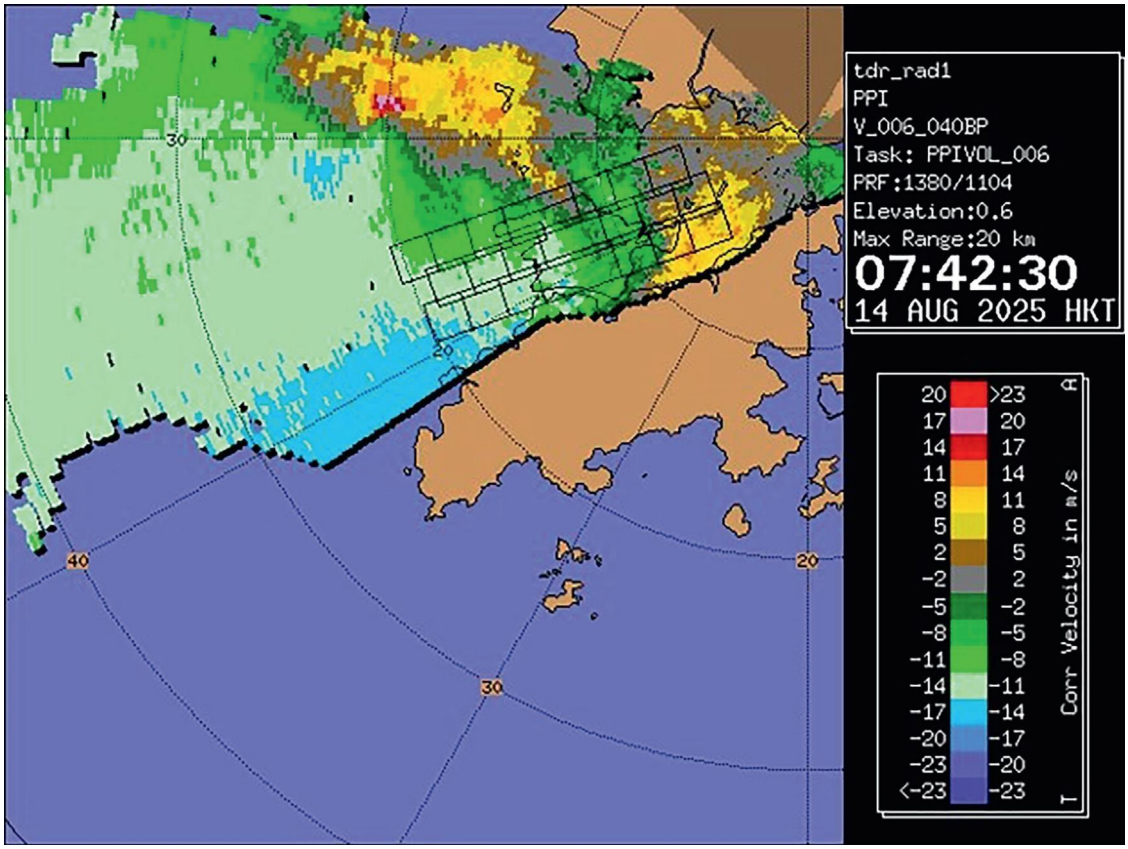

FIGURE 6: Doppler wind speed retrieved by Brothers Point TDWR at a 0.6-degree PPI scan at 23:42 UTC.

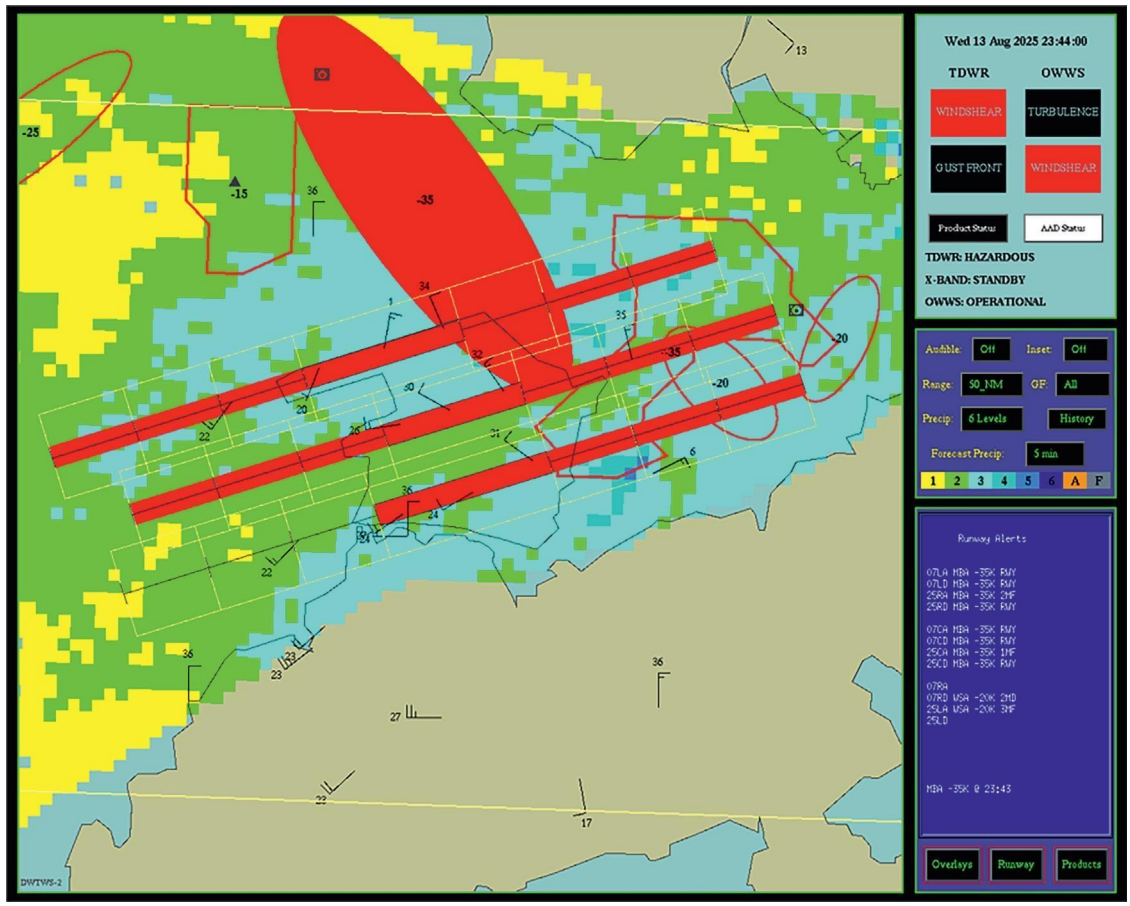

FIGURE 7: A snapshot of the WTWS display at 23:44 UTC. The solid red ellipse indicated the region of possible microburst alert based on the TDWR algorithm, and the hollow red ellipses showed regions of possible windshear.

Chen et al. [16], and the results are shown in Figure 11. The algorithm requires the input of three-dimensional wind data from the mesoscale model output, such as the Model for Prediction Across Scales (MPAS), at the specified layer and its neighboring layers to calculate the total kinetic energy and, hence, the EDR. In this study, the atmospheric model of UWIN-CM is the Weather Research and Forecasting Model (WRF) version 3.9. At the 925 and 940 hPa levels, the EDR could reach 0.5–0.6 $m^{2/3} s^{-1}$. This is not far from the aircraft observation in Figure 2a; values could potentially be higher or match the aircraft observation if the true magnitude of vertical wind can be accurately captured by the model.

7. Conclusion and Discussion

This is the first study of a microburst encounter by an aircraft near the surface of the HKIA, based on flight data, surface observations, weather radar data, and numerical simulation results. During this intense convective weather event, the major rainband contained several vortices in the lower troposphere. The aircraft flew through some of them and eventually conducted a missed approach because of the expectation of significant windshear (headwind loss near the ground) near the approach. It then encountered a microburst, with a clear updraft–downdraft couplet as shown in the aircraft data, the observations matched with the radar observations. The vertical cross section of the TDWR shows a couple of descending reflectivity cores, and this radar accurately provides microburst alerts to the airport.

In comparison to a typical intense microburst event that caused aircraft accident, taking Dallas/Fort Worth International Airport (DFW) microburst in 1985 [17] as an example, the microburst event discussed in this paper originated from multicell thunderstorms, while the case in DFW was triggered by an intense isolated cell. Ring vortices associated with a microburst were clearly identifiable in the DFW case, but the microburst structure in our case was likely disrupted by nearby convections within the multicell. The DFW case was far more intense, with damaging gusts up to 70 knots being reported near surface; and in our case, the maximum gusts near surface was below 30 knots based on anemometers over the aerodrome, but the headwind change of −35 knots

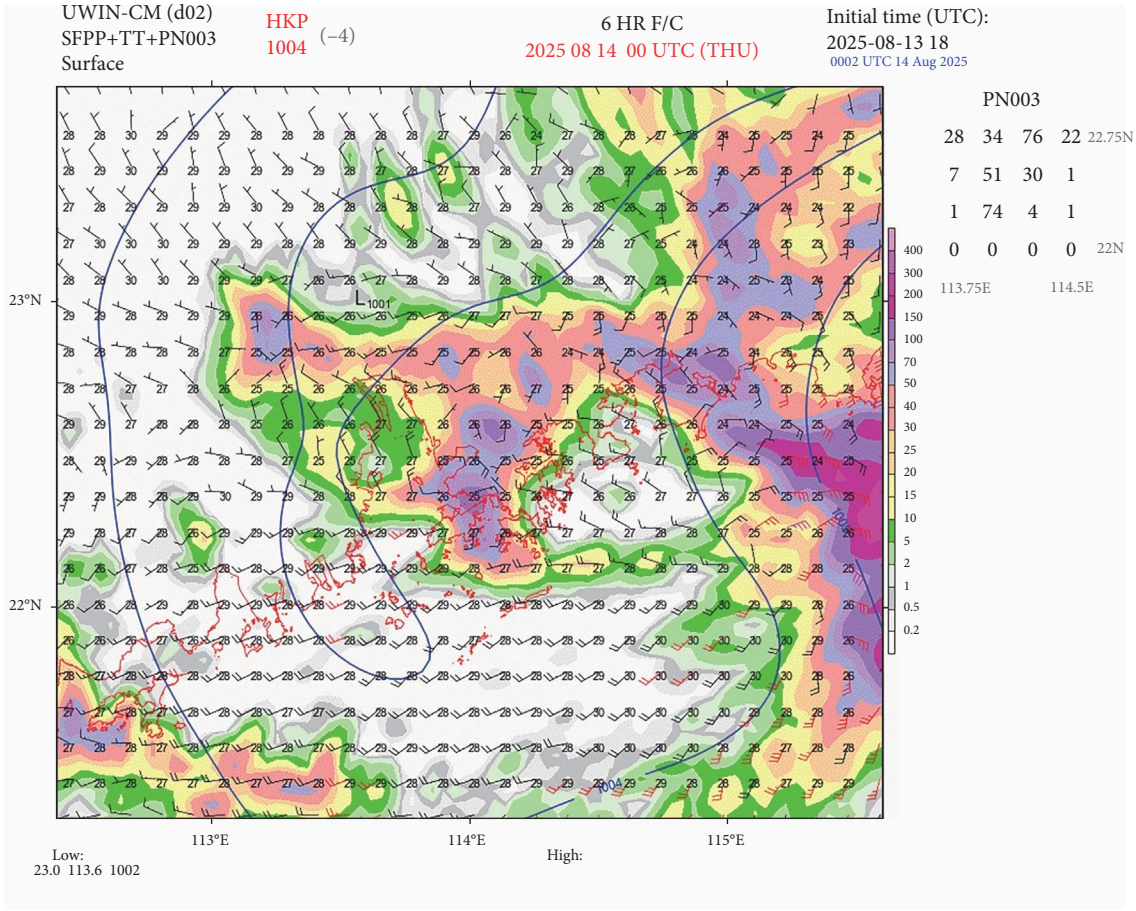

(a)

Figure 8: Continued.

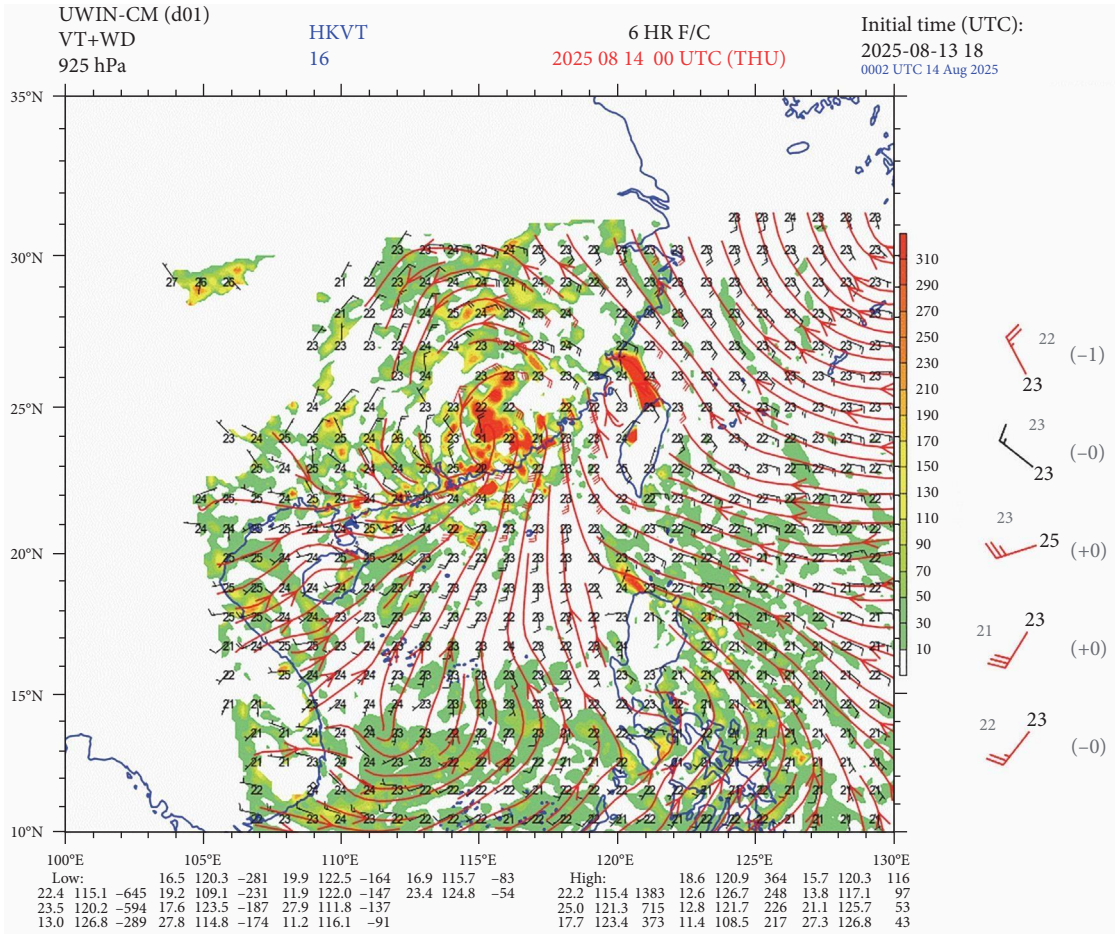

(b)

FIGURE 8: (a) Surface winds and 3-h accumulated precipitation; (b) 925 hPa winds and vorticity based on the T + 6 h forecast of the UWIN-CM model initialized at 18 UTC, August 13, 2025.

detected by TDWR was still significant enough to trigger the microburst alert. For the similarity of both cases, aircraft experienced an updraft followed by a downdraft upon their first encounter with microburst. It was fortunate that air traffic around HKIA was largely reduced on the morning of August 14 due to persistent convections in the vicinity, and the aircraft in this study conducted missed approach in advance, avoiding hard landing.

The convection-permitting NWP model, UWIN-CM, effectively captures downdrafts associated with intense convection, accompanied by updrafts on all sides. The EDR calculated from the NWP output indicated severe turbulence in association with intense convection near HKIA, but the values are slightly lower than the aircraft data and weather radar observations, likely because the magnitude of vertical winds at low levels is underestimated. Accurately forecasting the downdraft and EDR will be helpful for future developments in forecasting products related to windshear, microburst, and turbulence, to support aircraft operations.

The case presented in this paper is a single case study. More cases should be accumulated to better understand microbursts at HKIA and the technical feasibility of timely forecasting.

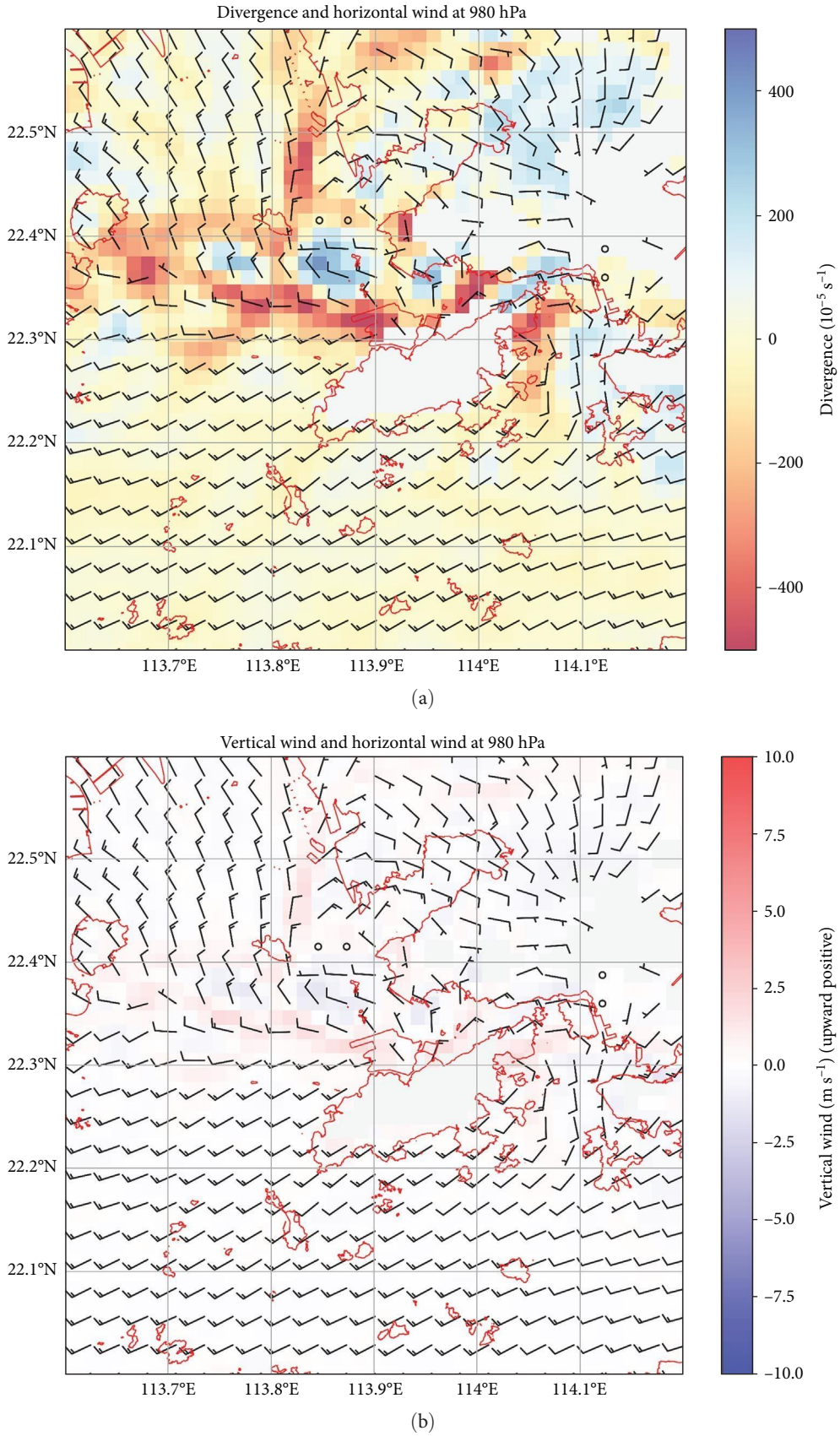

FIGURE 9: (a) Divergence and horizontal wind at 980 hPa; and (b) vertical wind and horizontal wind at 980 hPa based on the T + 6 h forecast of the UWIN-CM model initialized at 18 UTC, August 13, 2025.

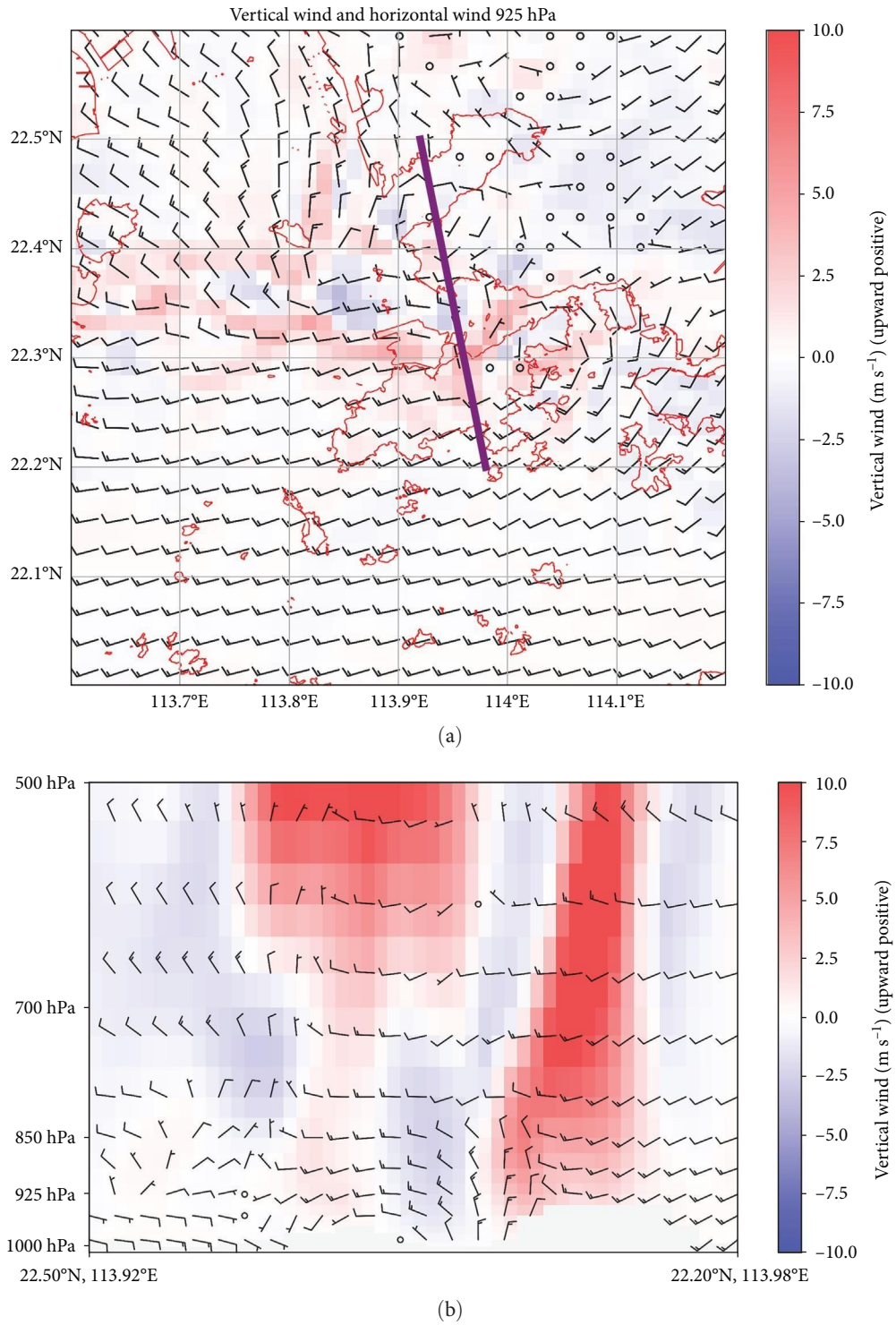

Figure 10: (a) Vertical wind and horizontal wind at 925 hPa; (b) the cross sectional horizontal and vertical winds along the purple line marked in (a) based on the T + 6 h forecast of the UWIN-CM model initialized at 18 UTC, August 13, 2025.

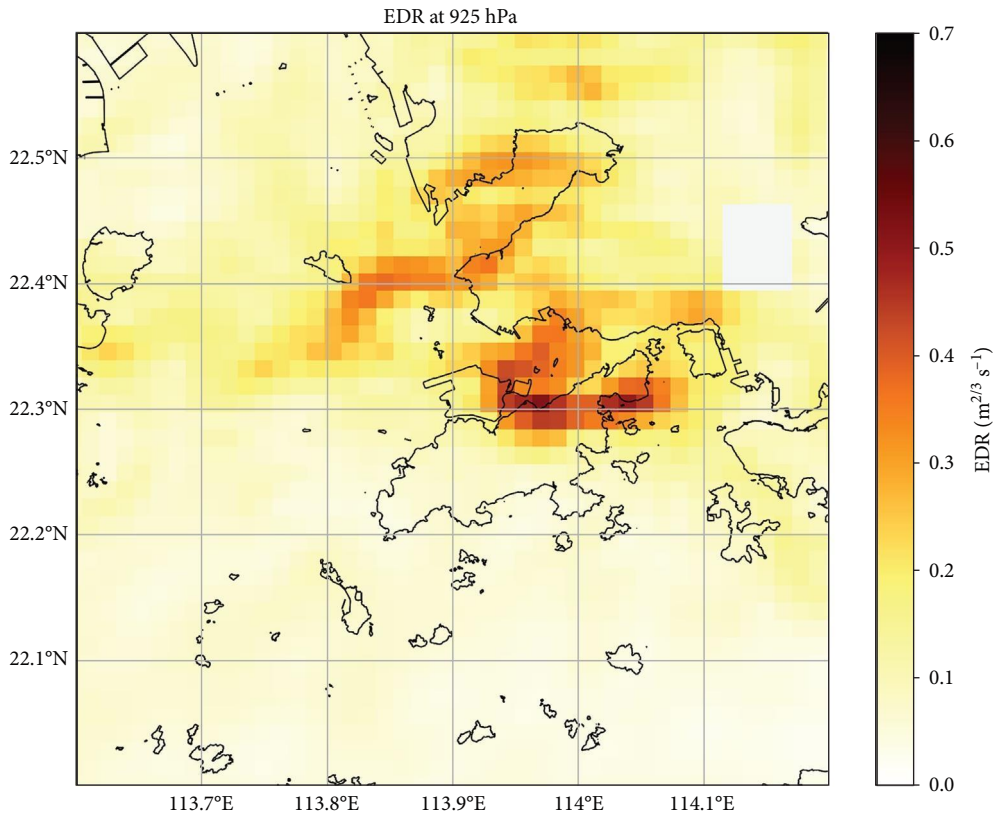

(a)

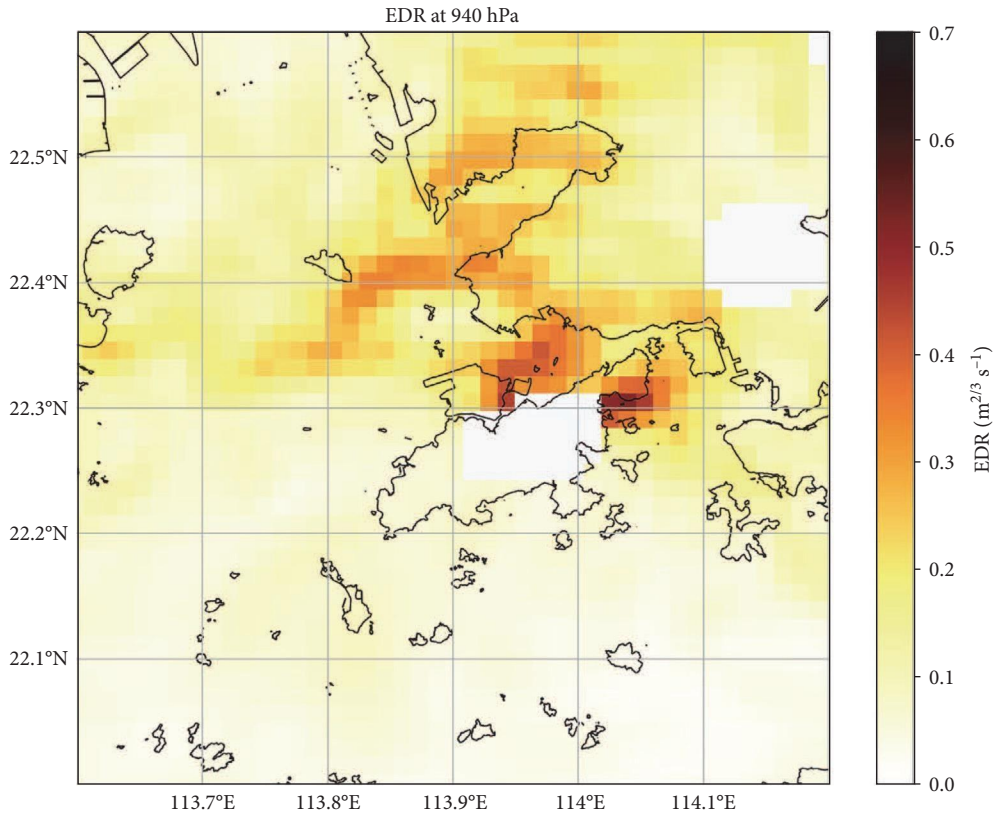

(b)

Figure 11: Continued.

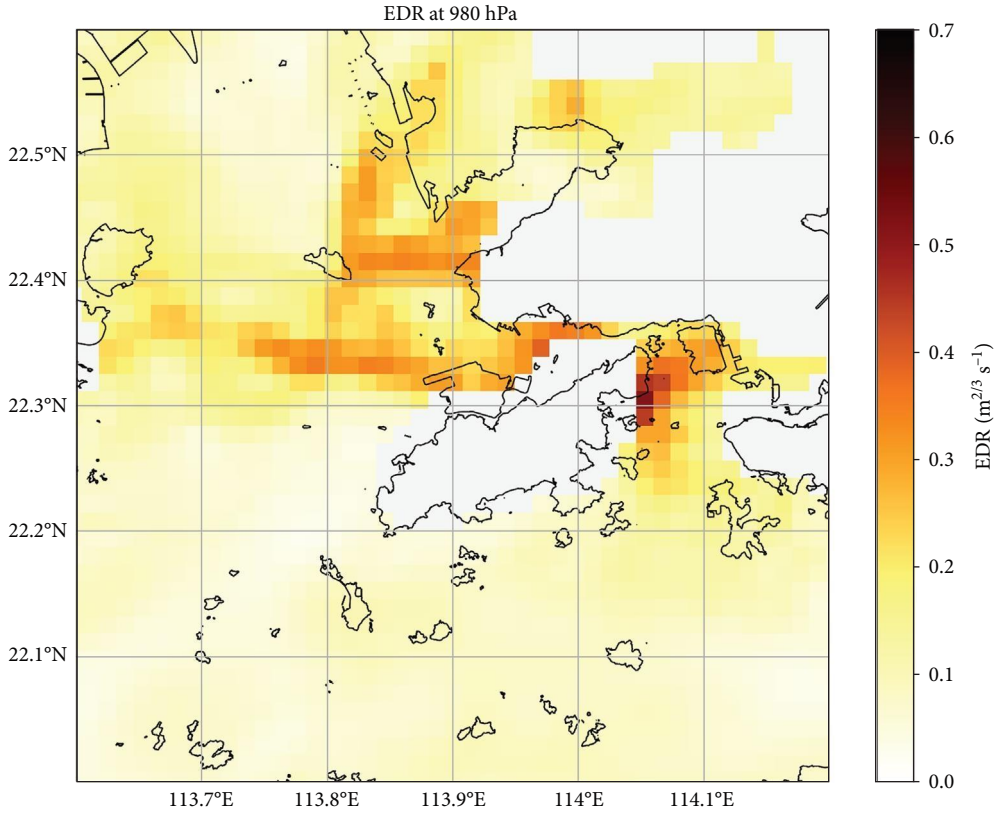

FIGURE 11: The model-derived EDR at (a) 925 hPa, (b) 940 hPa, and (c) 980 hPa based on the T + 6 h forecast of the UWIN-CM model initialized at 18 UTC, August 13, 2025.

Data Availability Statement

The data that support the findings of this study are available from the corresponding author upon reasonable request.

Conflicts of Interest

The authors declare no conflicts of interest.

Funding

No funding was received for this manuscript.

References

[1] G. A. Hookings, "Precipitation-Maintained Downdrafts," *Journal of Applied Meteorology* 4, no. 2 (1965): 190–195.

[2] R. C. Srivastava, "A Simple Model of Evaporatively Driven Dowadraft: Application to Microburst Downdraft," *Journal of the Atmospheric Sciences* 42, no. 10 (1985): 1004–1023.

[3] H. Pawłowska-Mankiewicz, "On the Role of Precipitation in Maintenance of Downdrafts in Cumulonimbus Clouds," *Atmospheric Research* 24, no. 1–4 (1989): 333–342.

[4] T. T. Fujita, "Tornadoes and Downbursts in the Context of Generalized Planetary Scales," *Journal of the Atmospheric Sciences* 38, no. 8 (1981): 1511–1534.

[5] T. T. Fujita, "The Downburst: Microburst and Macroburst," (University of Chicago, SMRP Research Paper 210, 1985).

[6] J. McCarthy, R. Serafin, J. Wilson, J. Evans, C. Kessinger, and W. P. Mahoney, "Addressing the Microburst Threat to Aviation: Research-to-Operations Success Story," *Bulletin of the American Meteorological Society* 103, no. 12 (2022): E2845–E2861.

[7] F. Caracena, J. McCarthy, and J. A. Flueck, "Forecasting the Likelihood of Microbursts along the Front Range of Colorado," *Conference on Severe Local Storms* 13 (1983): 261–264.

[8] H. Haverdings and P. W. Chan, "Quick Access Recorder (QAR) Data Analysis Software for Windshear and Turbulence Studies," *Journal of Aircraft* 47, no. 4 (2010): 1443–1447.

[9] S. H. Kim, J. Kim, J. H. Kim, and H. Y. Chun, "Characteristics of the Derived Energy Dissipation Rate Using the 1 Hz Commercial Aircraft Quick Access Recorder (QAR) Data," *Atmospheric Measurement Techniques* 15, no. 7 (2022): 2277–2298.

[10] R. Huang, H. Sun, C. Wu, C. Wang, and B. Lu, "Estimating Eddy Dissipation Rate with QAR Flight Big Data," *Applied Sciences* 9, no. 23 (2019): 5192.

[11] W. P. Mahoney and A. R. Rodi, "Aircraft Measurements on Microburst Development From Hydrometeor Evaporation," *Journal of the Atmospheric Sciences* 44, no. 20 (1987): 3037–3051.

[12] P. W. Chan, P. Zhang, and R. Doviak, "Calculation and Application of Eddy Dissipation Rate Map Based on Spectrum Width Data of an S-Band Radar in Hong Kong," *Mausam* 67, no. 2 (2016): 411–422.

[13] R. Jackson, S. Collis, T. Lang, C. Potvin, and T. Munson, "PyDDA: A Pythonic Direct Data Assimilation Framework for

Wind Retrievals," *Journal of Open Research Software* 8, no. 1 (2020): 20.

[14] T. K. Lau and Y. W. Chan, "Retrieval of 3D Wind Field Using Variational Multi-Doppler Wind Analysis for Studying High Impact Weather in Hong Kong," in *Proceedings of the 37th Guangdong-Hong Kong-Macao Seminar on Meteorological Science and Technology*, (Guangzhou, China, 03-13 https://www.weather.gov.hk/en/publica/reprint/files/r1825.pdf, 2025).

[15] P. W. Chan, K. K. Lai, W. Kong, and S. M. Tse, "Performance of Windshear/Microburst Detection Algorithms Using Numerical Weather Prediction Model Data for Selected Tropical Cyclone Cases," *Atmospheric Science Letters* 24, no. 9 (2023): e1173.

[16] H. Chen, C. Y.-Y. Leung, P. Cheung, H. Liu, S. T. Chan, and X. Shi, "Predicting Convectively Induced Turbulence With Regionally Convection-Permitting Simulations," *Asia-Pacific Journal of Atmospheric Sciences* 61, no. 2 (2025): 16.

[17] T. T. Fujita, "DFW Microburst," (University of Chicago, SMRP Research Paper No.217, 1986).